International Journal of Modern Physics B
Vol. 33, No. 6 (2019) 1950027 (9 pages)

DOI: 10.1142/S0217979219500279

World Scientific
www.worldscientific.com

Photoluminescence properties and threshold effect of ZnS:Ag nanoparticles synthesized by a hydrothermal process

Q. H. Li, S. P. Lin, D. C. Ma*,‡ and B. Wang†,‡
Sino-French Institute of Nuclear Engineering and Technology,
Sun Yat-sen University,
Guangzhou 510275, Guangdong, P. R. China
**madecai@mail.sysu.edu.cn*
†wangbiao@mail.sysu.edu.cn

Received 18 April 2018
Revised 6 November 2018
Accepted 5 December 2018
Published 26 February 2019

Ag-doped ZnS nanoparticles were prepared by hydrothermal synthesis from the raw powders of thiourea, zinc acetate and silver nitrate. The effects of Ag^+ on the structural, morphological, composition, elemental analysis and luminescence properties were investigated. The results showed that the powders were all found in the cubic sphalerite structure with an average particle size of approximately 40 nm. In addition, various Ag^+ doping concentrations (0, 0.5, 1, 3, 4, 7 and 10 at.%) were selected to study the optical properties of the ZnS nanoparticles. It was found that the photoluminescence (PL) spectra excited by 325 nm and X-ray showed a peak at 490 nm for all samples and exhibited concentration quenching behavior. The PL results also indicate that the most favorable silver doping concentration for emission is 3 at.%. These results suggested that ZnS:Ag (3 at.%) nanoparticles were promising candidate materials for certain areas, such as screen displays, scintillators and lasers.

Keywords: Ag-doped ZnS; hydrothermal route; nanoparticles; luminescence properties.

PACS numbers: 78.55.Et, 61.46.+w, 81.20.Ev

1. Introduction

Due to outstanding luminescence quality, nonlinear optical properties, quantum cutting, electrical properties and other excellent physical and chemical properties, research on luminescent II–VI group semiconductor materials has been performed in the past two decades for the application of these materials in integrated devices in a variety of fields, such as optical devices, conductors, sensors and diodes.[1–11]

[‡] Corresponding authors.

Zinc sulfide (ZnS), a promising group II–VI material, exists in nature mainly in the zinc blende and wurtzite structures with the direct bandgaps of 3.54 and 3.91 eV, respectively.[1,2] However, the pure ZnS cannot meet the demands of industrial application because its luminescence intensity is weak. When a small amount of transition metal ions, such as Ni, Mn, Co, Cu, Cd, Pb and Fe, is added to ZnS, the intensity of its fluorescent emission is improved and the emission wavelength can be adjusted. Furthermore, doped ZnS has good thermal and environmental stability. Doped ZnS semiconductor materials radiate visible light in different bands associated with various dopants. As the recombination centers for the electron-hole pairs, these transition metal ions doped into ZnS endow the material with strong characteristic photoluminescence. ZnS luminescence includes green emission from dopant Cu[8] and orange emission from dopant Mn.[12] Therefore, doped ZnS materials have strong prospects for applications in the fields of light emitting diodes, lasers, solar cells and biological markers.[13] ZnS nanoparticles doped with the transition metal ions can be synthesized using various techniques, such as co-precipitation, thermal evaporation, microwave, sol–gel processing, hydrothermal and microemulsions.[6–11] Among these methods, the hydrothermal method has become a popular approach due to its advantages of mild experimental conditions and ease of operation.

The optical properties of the ZnS:Ag nanocrystals are highly important for the applications of these materials. Several studies have already reported that different luminescence of ZnS:Ag is obtained using different synthetic methods, with the observed emission peaks being located at such wavelengths as 365, 450, 465, 494, 508, 522 and 544 nm.[14–18] In ZnS:Ag nanocrystals, the characteristic bands are also different from those reported in Refs. 18–21, where multiple emission bands were observed. The blue-green emissions of Ag-doped ZnS crystals are also observed in Ref. 22. In these works, the hydrothermal process was utilized to syntheses Ag-doped ZnS with zinc acetic, thioacetamide and silver nitrate.[14,15] The emission peaks are located at about 460 nm. The luminescence intensities were enhanced with the increase of Ag^+ ions concentration but no threshold effect was observed because the Ag^+ ions concentrations are no more than 2%. In the present work, we synthesized the ZnS:Ag nanoparticles by using the hydrothermal method with zinc acetic, thiourea and silver nitrate. The effects of various Ag^+ ions concentration (0, 0.5, 1, 3, 4, 7 and 10 at.%) on the luminescence properties were studied. It was found that ZnS:Ag show an emission peak at 490 nm and threshold effects. Furthermore, the enhanced blue luminescence is observed in ZnS:Ag nanoparticles. This finding suggests that Ag^+-doped (3 at.%) ZnS nanoparticles have maximal emission efficiency.

2. Experimental

Ag-doped (0, 0.5, 1, 3, 4, 7 and 10 at.%) ZnS nanoparticles were synthesized by the hydrothermal process. The experiments are performed in an aqueous solution in a vacuum glove box. Zinc acetic (Aladdin, 99.99%) and thiourea (Aladdin, AR) were added in deionized water and stirred for 10 min in order to obtain homogeneous solutions, respectively. In these two types of solutions, the concentration of zinc acetic and thiourea are 0.25 and 0.6 mol/L, respectively. The $AgNO_3$ solution (Aladdin, AR) (0.005, 0.01, 0.03, 0.04, 0.07 and 0.10 mol/L) was prepared by dissolving it in deionized water. Next, the zinc acetic and thiourea solution were mixed and stirred for 5 min. The silver nitrate solution was added last and made the mixture rapidly change from colorless and clear to brown and opaque. Finally, the mixed solution was transferred to a high-pressure autoclave with a volume fraction of 80%. The high-pressure autoclave was maintained at 230°C for 15 h and was naturally cooled to room-temperature (RT). After separation by centrifuging, the ZnS:Ag nanoparticles were rinsed alternately with de-ionized water and alcohol. The separated powder was dispersed in alcohol by ultrasound for approximately 10 min in an ultrasound shaker. The powder was dried at 70°C for 6 h in a vacuum oven after several cycles. To prepare undoped ZnS nanoparticles, the same procedure was used as that used for the preparation of Ag-doped ZnS, except that the silver nitrate solution was replaced by the same volume of de-ionized water.

The phase structures of the obtained powders were measured by X-ray diffraction (XRD) in the 2θ range from 20° to 80° using a D-MAX 2200 VPC instrument with Cu $K\alpha 1$ radiation ($\lambda = 1.54206$ Å), step-scanning with a step size of 0.02° and a scanning rate of 10°/min. The sizes and morphology of the samples were acquired using a JEM-2010 HR transmission electron microscope (TEM). Emission and excitation spectra were recorded using an EDINBURGH INSTRUMENTS LTD FLSP920 spectrophotometer and under irradiation by an ENERGETIQ EQ-1500 used as the light source. The X-ray excited optical luminescence (XEOL) spectra were acquired using the MAGPRO X-ray Source (50 KV, 100 μA) to excite the Ag-doped ZnS nanoparticles. The X-ray photoelectron spectrometry (XPS) analysis of Ag-doped ZnS nanoparticles was performed using a Thermo SCIENTIFIC ESCALAB 250Xi instrument. The Ag^+ contents were analyzed using an Agilent 5100 inductive coupled plasma (ICP) emission spectrometer.

3. Results and Discussion

Figure 1 shows the ZnS:Ag nanoparticles XRD patterns for different Ag^+ concentration. In this figure, the three stronger peaks at 28.57°, 47.52° and 56.40° were due to the cubic crystalline structure (JCPDS Card, File No.050566),[23] consistent with the {1 1 1}, {2 2 0} and {3 1 1} planes of the zinc blende phase, respectively. No significant phases other than zinc sulfide are found in all of the samples, indicating that Ag^+ ions were successfully incorporated into ZnS, thereby leading to a slight effect on the patterns. From the XRD results, the lattice constant $a = 5.30$ Å is obtained. Accordingly, the average gain size L can be evaluated by $L = k\lambda/\beta cos\theta$,[24] where k is the shape factor (spherical approximately 1.0); λ the X-ray wavelength (0.154206 nm); β is the characteristic line-width of the diffraction peak; and θ is the Bragg diffraction angle. As listed in Table 1, the grain sizes decreases with the increasing Ag^+ concentration.

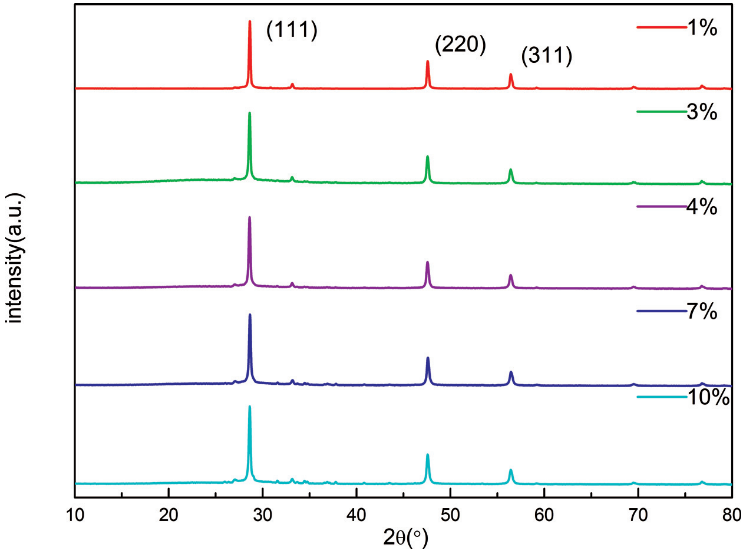

Fig. 1. (Color online) XRD patterns of the ZnS:Ag nanoparticles. ($K = 1, \lambda = 0.154206$ nm).

Table 1. Calculated sizes of ZnS:Ag nanoparticles synthesized with various Ag^+ doping concentration ($K = 1, \lambda = 0.154206$ nm).

Ag^+ concentration	1%	3%	4%	7%	10%
L (nm)	43.61	41.46	41.04	38.82	38.16

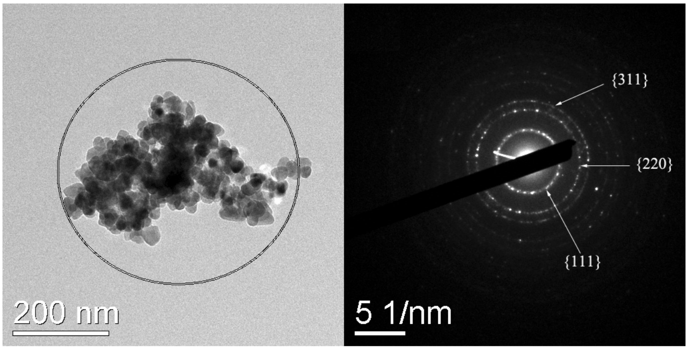

(a) (b)

Fig. 2. TEM image of the ZnS:Ag (3 at.%) nanoparticles and its electron diffraction pattern.

The TEM image and electron diffraction pattern of ZnS:Ag (3 at.%) nanoparticles are presented in Fig. 2. The TEM image in Fig. 2(a) indicates that the powders are nearly spherical particles. The particle sizes measured from the TEM image is approximately 39 nm. This result is in good agreement with the expectation from

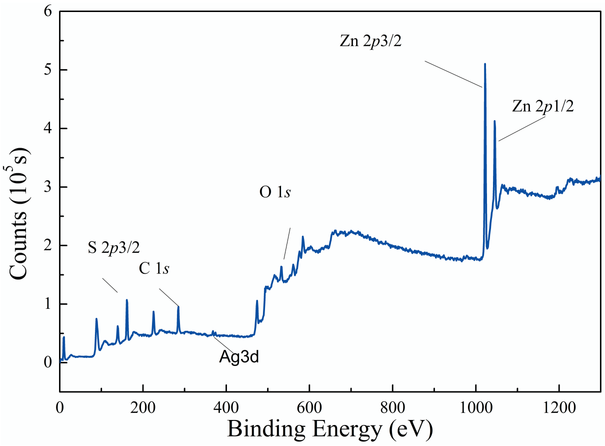

Fig. 3. (Color online) XPS spectrum of the ZnS:Ag (3 at.%) nanoparticles.

the XRD measurement results. As seen in Fig. 2(b), three concentric rings that are shown from the selected area electron diffraction pattern correspond to the {1 1 1}, {2 2 0} and {3 1 1} plane diffractions of the ZnS cubic structure inside and outside.

Figure 3 shows the XPS spectrum of the Ag-doped (3 at.%) ZnS nanoparticles. It is observed from the figure that not only the peaks of Ag, S, Zn are present but also the peaks of other elements, such as O (O 1*s*, 531.8 eV) and C (C 1*s*, 285.03 eV) that are due to the precursor and the natural environment, respectively. It is observed from Fig. 3 that the Zn 2*p*3/2 and Zn 2*p*1/2 peaks are located respectively at 1022.17 and 1045.17 eV, due to the corresponding excited states of ZnS.[25–27] Moreover, the peak located at 161.97 eV is due to the binding energy of S 2*p* in the typical sulfide.[28] In addition, it is deduced from the XPS results that the Zn/S molar ratio of Ag (3 at.%):ZnS is 0.863. The Zn/S molar ratio of undoped ZnS is 0.9043, which is bigger than that of Ag (3 at.%):ZnS. The result shows silver ions are doped into ZnS and replace some of the zinc so the ratio of zinc to sulfur decreased. It also indicates that Zn is the smaller component in the ZnS:Ag nanoparticles.

In Fig. 4 the ICP results shows the Ag^+ concentration in the as synthesized ZnS nanoparticles comparing with that in the raw solutions. The Ag^+ concentration in the ZnS nanoparticles is less than that of raw solution because the Ag^+ ions suffered segregation in the solution during the formation of ZnS:Ag nanoparticles. The Ag^+ concentration of the ZnS nanoparticles is 2.27 at.% while the Ag^+ concentration is 3% in the raw solution.

Figure 5 shows the influence of various Ag^+ concentrations on the excitation and emission spectra of the ZnS nanoparticles. The measurements of the photoluminescence spectra were performed with 355 nm excitation at RT, respectively. An optical filter was inserted in front of the samples to block any light having wavelengths above 380 nm. It is observed from Fig. 5(a) that the PL spectra of the ZnS:Ag

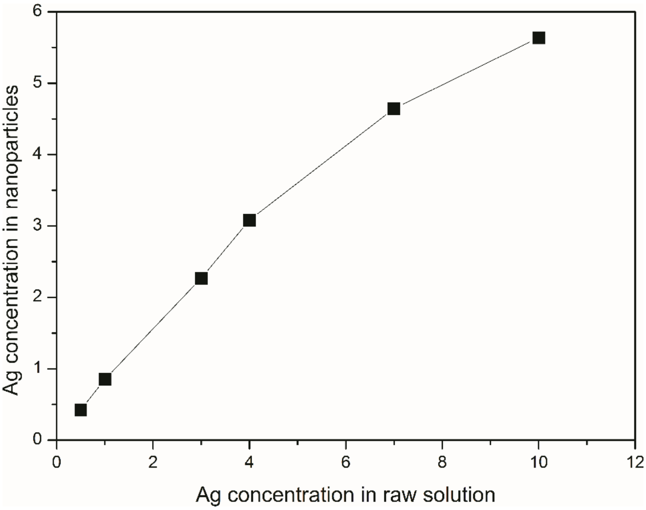

Fig. 4. The Ag^+ concentration in the ZnS nanoparticles for different doping concentration in the raw solution.

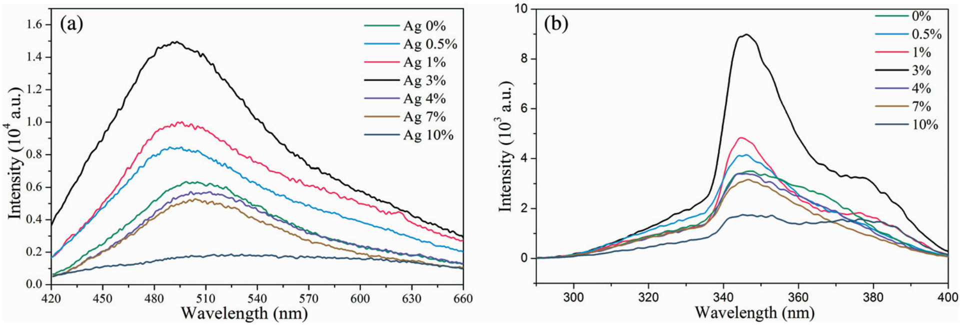

Fig. 5. (Color online) (a) Emission spectra and (b) excitation spectra of the ZnS:Ag nano-particles.

nanoparticles show a broadband spectrum, ranging from 400 to 580 nm and centered at approximately 490 nm. The emission peaks of the Ag-doped ZnS were also observed in previous work,[5,20,22] different from the results reported in Refs. 16–19. It is well-known that in ZnS there are four types of photoluminescent point defects, namely, interstitial S, interstitial Zn, S vacancy and Zn vacancy. Based on their energies, the emission peaks are speculated to be due to the Zn vacancy (489 nm), S vacancy (427 nm), interstitial Zn (385 nm) and interstitial S (349 nm),[29–33] From the XPS results, it is found that the ZnS nanoparticles prepared in the present work are Zn-poor. When silver is incorporated alone, the observed self-activated emission is associated with a complex luminescent center, such as $(V_{Zn}–Ag_{Zn})^-$.[30,34] As the Ag^+ concentration increases, the intensity of the emission peaks first increases and then decreases. The emission peaks shift slightly compared to pure ZnS

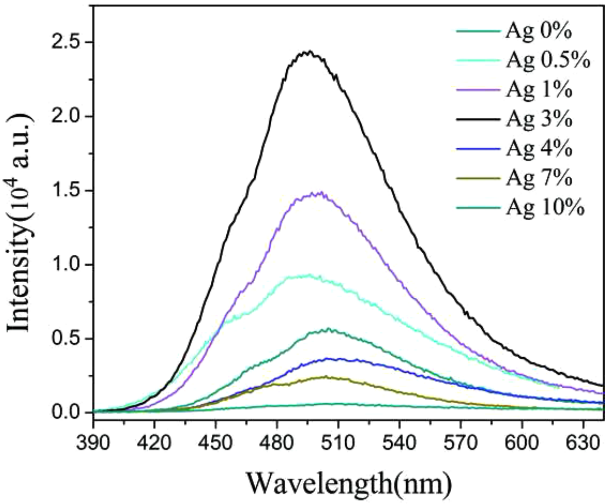

Fig. 6. (Color online) Emission spectra of the ZnS:Ag nanoparticles excited by X-ray excitation at RT.

nanoparticles. In addition, the ZnS:Ag^+ nanoparticles present a threshold value at the Ag^+ concentration of 3%. When the doping concentration is less than 3%, the emission peak intensity increases with increasing silver doping concentration. Subsequently, the luminous intensity decreases with increasing concentration of Ag^+ in the ZnS nanoparticles, which can be interpreted as the concentration quenching effect.

Figure 5(b) shows that the exciting peak at 355 nm is the band-edge absorption of ZnS.[35] When the doping concentration is more than 3%, the exciting peak drops down with the increasing Ag^+ concentration in the ZnS nanoparticles.

Figure 6 shows the luminescence spectra of the ZnS:Ag nanoparticles excited by the X-ray (50 KV and 100 μA) irradiation. As observed from Fig. 6 the XEOL spectra show good agreement with the PL spectra shown in Fig. 4(a). The intensity of the emission peaks first increases and then decreases with increasing Ag^+ concentration. The ZnS:Ag^+ nanoparticles present a threshold value at the Ag^+ concentration of 3%. But the peak width decreases slightly compared to the PL spectra and the luminous intensity of Ag^+ concentration 3 at.% is almost 5 times as against pure ZnS. The XEOL results are attributed to the recombination between the Zn vacancy ($(V_{Zn}–Ag_{Zn})^-$) related electron trap donor below the conduction band and the valence band.

The diffusion of Ag^+ within the zinc sulfide matrix is promoted by high-temperature and pressure conditions in the hydrothermal reaction. Consequently, the intensity of Ag^+ luminescent center becomes stronger. Conversely, the diffusion of Ag^+ may lead to crystal defects in the zinc sulfide matrix, such as zinc vacancies. For a low Ag^+ concentration, diffusion of Ag^+ in the zinc sulfide matrix is weak. Only a small amount of zinc vacancies are generated, which has a beneficial impact on the luminous intensity. Therefore, the luminous capacity of ZnS:Ag nanoparticles is enhanced with increasing silver doping. As mentioned above, the most favorable silver doping concentration for emission is 3 at.%. Next, the luminous intensity decreases as the Ag^+ concentration increases in ZnS nanoparticles. The reasons for this finding are as follows: (1) Zn vacancy content also increases sharply, resulting in a loss of a large amount of energy during the transmission process[36]; and (2) More Ag_2S will be produced as the Ag^+ concentration in the sulfide matrix is increased. The Ag_2S nanoparticles play the role of nonradiative recombination centers,[15,18] the intensity of emission decreases. As a result, the luminous intensity of the Ag:ZnS nanoparticles decreases.

4. Conclusion

Ag-doped ZnS nanoparticles were synthesized using solutions of zinc acetic, thiourea and silver nitrate by the hydrothermal process. The ZnS:Ag nanoparticles are all found in a sphalerite structure, and their grain sizes are approximately 40 nm. The PL spectra and XEOL spectra show that emission peaks of ZnS:Ag is located at approximately 490 nm rised from Zn vacancy, and the concentration quenching effect is observed in the Ag-doped ZnS nanoparticles. This finding suggests that the most favorable silver doping concentration for emission of the ZnS:Ag nanoparticles is 3 at.% in raw solution corresponding to 2.27 at.% in the generated powders by hydrothermal process. Therefore, our results indicate that the Ag^+ (3 at.%)-doped ZnS nanoparticles may have great potential applications in scintillators, screen displays, lasers and other devices.

Acknowledgments

This work was supported by the National Natural Science Foundation of China (NSFC) (Nos. 11372361, 11302268, 11232015, 11472321 and 11572355).

References

1. S. Ferahtia, S. Saib and N. Bouarissa, *Int. J. Mod. Phys. B* **30**, 1650147 (2016).
2. K. A. Guzmán-Garcíaa *et al.*, *Radiat. Meas.* **107**, 58 (2017).
3. A. Bahari and Z. S. Soltani, *Int. J. Mod. Phys. B* **26**, 1250074 (2012).
4. T. Kang, J. Sung and W. Shim, *J. Phys. Chem. C* **113**, 5352 (2009).
5. C. F. Wang, Q. S. Li and B. Hu, *Int. J. Mod. Phys. B* **31**, 1744055 (2017).
6. B. S. Rao *et al.*, *Chalcogenide. Lett.* **177**, 8 (2011).
7. S. J. Xu *et al.*, *Appl. Phys. Lett.* **73**, 478 (1998).
8. H. Hu and W. Zhang, *Opt. Mater.* **28**, 536 (2006).
9. N. Karar, F. Singh and B. R. Mehta, *J. Appl. Phys.* **95**, 656 (2004).
10. C. H. Ye *et al.*, *Appl. Phys. Lett.* **85**, 3035 (2010).
11. W. Chen *et al.*, *Phys. Rev. B* **61**, 11021 (2000).
12. W. Q. Peng *et al.*, *J. Cryst. Growth* **282**, 179 (2005).
13. X. Duan *et al.*, *Nature* **409**, 66 (2001).
14. H. Qu *et al.*, *Adv. Mater. Res.* **79–82**, 589 (2009).

15. D. Z. Qin *et al.*, *Chalcogenide Lett.* **9**, 441 (2012).
16. H. M. Yang *et al.*, *J. Alloys. Compd.* **402**, 274 (2005).
17. V. Ramasamy, K. Praba and G. Murugadoss, *Spectrochim. Acta A* **96**, 963 (2012).
18. E. Shahriari *et al.*, *Opt. Quant. Electron.* **49**, 151 (2017).
19. K. B. Lin and Y. H. Su, *Appl. Phys. B* **113**, 351 (2013).
20. K. Patel, M. P. Deshpande and S. H. Chaki, *Appl. Phys. A* **123**, 367 (2017).
21. R. Sarkar, P. Kumbhakar and A. K. Mitra, *NSTI-Nanotech* **1**, 343 (2011).
22. X. X. Luo, W. H. Cao and L. X. Zhou, *J. Lumin.* **122**, 812 (2007).
23. S. Kumar, N. K. Verma and M. L. Singla, *Mater. Chem. Phys.* **142**, 734 (2013).
24. M. Shamsipur *et al.*, *Mat. Sci. Semicon. Proc.* **16**, 1154 (2013).
25. B. Elidrissi *et al.*, *Mat. Chem. Phys.* **68**, 175 (2001).
26. X. Yang *et al.*, *ACS Appl. Mater. Inter.* **6**, 9078 (2014).
27. W. D. Shi *et al.*, *Appl. Catal. B-Environmental* **138–139**, 184 (2013).
28. L. H. Yu *et al.*, *Appl. Catal. B-Environmental* **164**, 453 (2015).
29. D. Denzler, M. Olschewski and K. Sattler, *J. Appl. Phys.* **84**, 2841 (1998).
30. M. V. Limaye *et al.*, *Nanotechnology* **19**, 415602 (2008).
31. N. Kumbhojkar *et al.*, *J. Appl. Phys.* **88**, 6260 (2000).
32. S. Wageh, S. L. Zhao and X. R. Xu, *J. Cryst. Growth* **255**, 332 (2003).
33. S. L. Shen *et al.*, *Angew. Chem.* **123**, 7253 (2013).
34. A. Ortiz, J. C. Alonso and V. Pankov, *J. Mater. Sci.-Mater. El.* **10**, 503 (1999).
35. H. Qu *et al.*, *J. Appl. Phys.* **106**, 093506 (2009).
36. D. Y. Jiang *et al.*, *Nucl. Sci. Tech.* **28**, 32 (2017).